ELSEVIER

Journal of Photochemistry and Photobiology A: Chemistry 152 (2002) 109–121

Journal of Photochemistry and Photobiology A:Chemistry

www.elsevier.com/locate/jphotochem

# Kinetic studies of the photoinitiated NO-releasing reactions of *N*,*N*′-bis-(carboxymethyl)-*N*,*N*′-dinitroso-1,4-phenylenediamine

Maria Zulema Cabail, Peter Jon Lace, John Uselding, A. Andrew Pacheco*

*Department of Chemistry, University of Wisconsin-Milwaukee, Milwaukee, WI 53211, USA*

Received 21 December 2001; received in revised form 17 May 2002; accepted 28 May 2002

**Abstract**

Irradiation of *N*,*N*′-bis-(carboxymethyl)-*N*,*N*′-dinitroso-1,4-phenylenediamine (**1**) with ultraviolet light ($\lambda = 308$ nm) was previously shown to induce cleavage of **1** into NO and the *N*,*N*′-bis-(carboxymethyl)-*N*-nitroso-1,4-phenylenediamine radical (**2**). This paper provides a procedure for synthesizing **1**, and a detailed kinetic re-investigation of the reactions that follow ns-pulse laser-flash photolysis of **1**, under conditions that initially produce up to 10 μM of **2** and NO in situ. Under these conditions recombination of **2** with NO, and dissociation of an additional equivalent of NO from **2**, appear to be the dominant pathways leading to the depletion of **2** in the ms that follows the initial photolysis. These reactions had been suggested in the initial study of the photolysis of **1**; however, in the present study the rate constant $k_r$ that governs the recombination of **2** with NO to regenerate **1** was found to have a value of $(1.1 \pm 0.1) \times 10^9\ M^{-1}\ s^{-1}$, while the rate constant $k_d$ governing the dissociation of the second equiv of NO from **2** was found to be $500 \pm 50\ s^{-1}$. Both of these values are significantly different from the values ($1.38 \times 10^8\ M^{-1}\ s^{-1}$ and $2.96 \times 10^4\ s^{-1}$) reported in the earlier study. The present analysis also revealed the previously unreported presence of an absorbing species at $t_\infty$, that might be the doubly denitrosylated quinoimine derivative of **1** (**3**), or a charge-transfer complex of **1** and **3**.


*Keywords:* *N*,*N*′-Bis-(carboxymethyl)-*N*,*N*′-dinitroso-1,4-phenylenediamine; Synthesis; Nitric oxide generation; Kinetics; Mechanism

## 1. Introduction

Since the early 1990s nitric oxide has been recognized to have important physiological roles as a vascular regulator, in neuronal communication, and as a cytotoxic agent in the immune system [1–6]. This has stimulated intense interest in all aspects of the chemistry and biochemistry of NO and its derivatives [7–12]. One particular area of interest has been the design and synthesis of biologically inert precursor compounds, that can be activated to release NO once they reach specific biological target sites [13–17]. *N*,*N*′-Bis-(carboxymethyl)-*N*,*N*′-dinitroso-1,4-phenylenediamine (**1**) is one such compound, that releases 2 equiv of NO upon photoactivation with 308 nm light (Scheme 1) [14,17,18].

Though designed for their potential biomedical applications, compounds such as **1** can also be used as valuable research tools. NO can be generated from **1** in less than 1 μs using a XeCl excimer laser, so very fast subsequent reactions of NO with other compounds can be monitored [14,17]. The concentration of NO within a given experiment is readily controlled, either by varying the intensity of the laser pulse, or by maintaining the laser pulse constant and varying the concentration of **1**. Scheme 1 illustrates the mechanism for NO generation that was proposed by Namiki et al. [14], when they first presented this methodology. The initial laser flash causes the dissociation of 1 equiv of NO from **1**, and also produces **2**, which is detectable by its transient UV absorbance spectrum ($\lambda_{max} \sim 400$ nm) [14]. Compound **2** subsequently disappears, as evidenced by the decrease in $A_{400}$, which is believed to occur via two pathways (Scheme 1): the recombination of NO with **2** to regenerate **1**, and the dissociation of a second equiv of NO to generate **3**.

We are investigating the ability of NO to selectively reduce the active site of the enzyme hydroxylamine oxidoreductase by $1e^-$, and have found **1** to be a highly versatile reagent for this endeavor [19]. For our purposes it is critical to know the exact concentration of NO that is generated under a given set of conditions, and this led us to re-examine in detail the reaction kinetics of the process depicted in Scheme 1. We have found a substantial discrepancy between our value of $k_d$ (Scheme 1) and the previously published value, and a

* Corresponding author. Fax: +1-414-229-5530.
*E-mail address:* apacheco@uwm.edu (A.A. Pacheco).

1010-6030/02/$ – see front matter © 2002 Elsevier Science B.V. All rights reserved.
PII: S1010-6030(02)00231-9

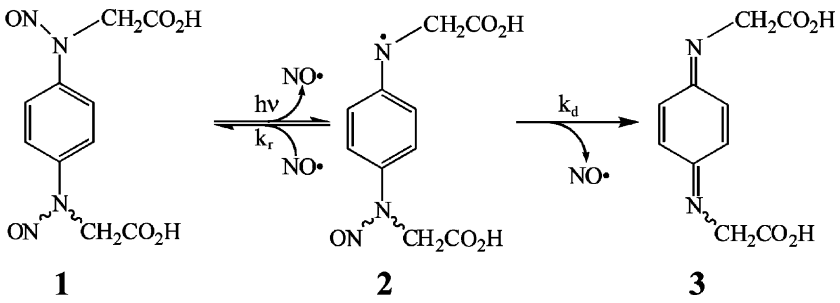


Scheme 1.

smaller difference between our value of $k_r$ and the published value [14]. Herein we describe our kinetic analysis, which also brings to light other previously unreported observations. We also describe the synthesis of **1**, which has not previously been reported in detail.

## 2. Experimental section

### 2.1. Synthesis, general considerations

Anhydrous *N*,*N*′-dimethylformamide (DMF) was obtained from ACROS, packed under nitrogen in septum-sealed bottles. *N*,*N*′-Diacetyl-1,4-phenylenediamine (98%) (**4**) was obtained from Lancaster as a greyish powder. NaH was a 60% dispersion in paraffin oil, obtained from ACROS; prior to use, the protecting paraffin oil was removed from the NaH by washing with *n*-heptane and THF. All other reagents were obtained from Fisher or ACROS, and were reagent grade. Compound **1** was synthesized in two steps as described below, according to the general outline described by Namiki et al. [14] (Scheme 2). Both the intermediate *N*,*N*′-bis-( carbethoxymethyl )-*N*,*N*′-diacetyl-1,4-phenylenediamine, **5** (Scheme 2), and **1** were synthesized under a nitrogen atmosphere. Once synthesized **5** is air-stable, and its purification by column chromatography and recrystallization was carried out without special precautions. Target compound **1** is also relatively air-stable in the short term, but was stored under nitrogen to avoid long-term oxidation.

### 2.2. *N*,*N*′-Bis-(carbethoxymethyl)-*N*,*N*′-diacetyl-1, 4-phenylenediamine (*5*)

To a solution of 5 g (26 mmol) of **4** in 100 ml DMF were added 1.25 g (52 mmol) of NaH. The resulting dark-purple suspension was heated to 90 °C with vigorous stirring, and became progressively lighter colored and gelatinous. After about 20 min the purple gelatinous material was removed from heat and cooled to 5 °C in an ice bath, after which 7.5 ml (8.7 g, 70 mmol) of ethyl chloroacetate were added dropwise while stirring vigorously. The gelatinous precipitate dissolved rapidly upon addition of the ethyl chloroacetate, leaving a brown solution that contained a greyish suspension of particulate matter. About half of the DMF was removed by rotary evaporation at 65 °C, then the suspension was centrifuged in Teflon centrifuge tubes to remove NaCl. The remaining DMF was removed from the supernatant by further rotary evaporation, then the solid was resuspended in 30 ml of chloroform, and centrifuged to remove starting material and residual NaCl. The supernatant was filtered to remove residual solid, dried to a thick syrup using rotary evaporation, then re-dissolved in minimal chloroform and added to a 50 ml silica column (Davisil Type 150A, 100–200 mesh, grade 644) equilibrated with 1:1 toluene/chloroform. Pure **5** eluted from the column in 1:1–1:2 toluene/chloroform, and recrystallized from toluene as a white powder. Yield: 10%, with the remainder being mostly starting material **4** and the mono-carbethoxymethyl phenylenediamine derivative (containing traces of **5**). These could be readily separated from each other by chromatography, and later used to obtain more pure **5**. UV–Vis ($\lambda_{max}$, $\varepsilon_{max}$ $mM^{-1}$ $cm^{-1}$, in methanol): (238, 9.2). $^1$H NMR ($\delta$, m, in $CDCl_3$): 1.30, t, 6H of $RCOOCH_2(CH_3)$; 1.97, s, 6H of $R_2$ $R_3NCO(CH_3)$; 4.20, q, 4H of $RCOO(CH_2)CH_3$; 4.38, s, 4H of $R_2R_4N(CH_2)COOEt$; 7.43, s, 4H of Ph ring. Mass spectroscopy (*m*/*z*, EI): 364 [$M^+$].

### 2.3. *N*,*N*′-Bis-(carboxymethyl)-*N*,*N*′-dinitroso-1, 4-phenylenediamine (*1*)

To 50 ml of a 10% $H_2SO_4$ solution were added 0.509 g (1.4 mmol) of **5**. The suspension was thoroughly degassed for 1 h under a nitrogen purge, during which time most of the solid dissolved, presumably due to hydrolysis of the ester linkage. The solution was then heated and stirred under reflux conditions for 2 h, after which it was cooled to 4 °C in an ice bath. At this point 10 ml of a degassed 0.3 M $NaNO_2$ solution were added (2.8 mmol $NaNO_2$), which evoked an immediate intense pink color from the reaction mixture. This pink color disappeared within less than a minute, and was replaced by a pale yellow precipitate. The precipitate was filtered, washed with multiple aliquots of ice-cold deionized water to remove acid and an unidentified yellow soluble side-product ($\lambda_{max}$ = 375 nm), then dried under vacuum overnight. Yield: 0.303 g (1.07 mmol), 76%. UV–Vis ($\lambda_{max}$, nm, $\varepsilon_{max}$, $mM^{-1}$ $cm^{-1}$, in 25 mM phosphate

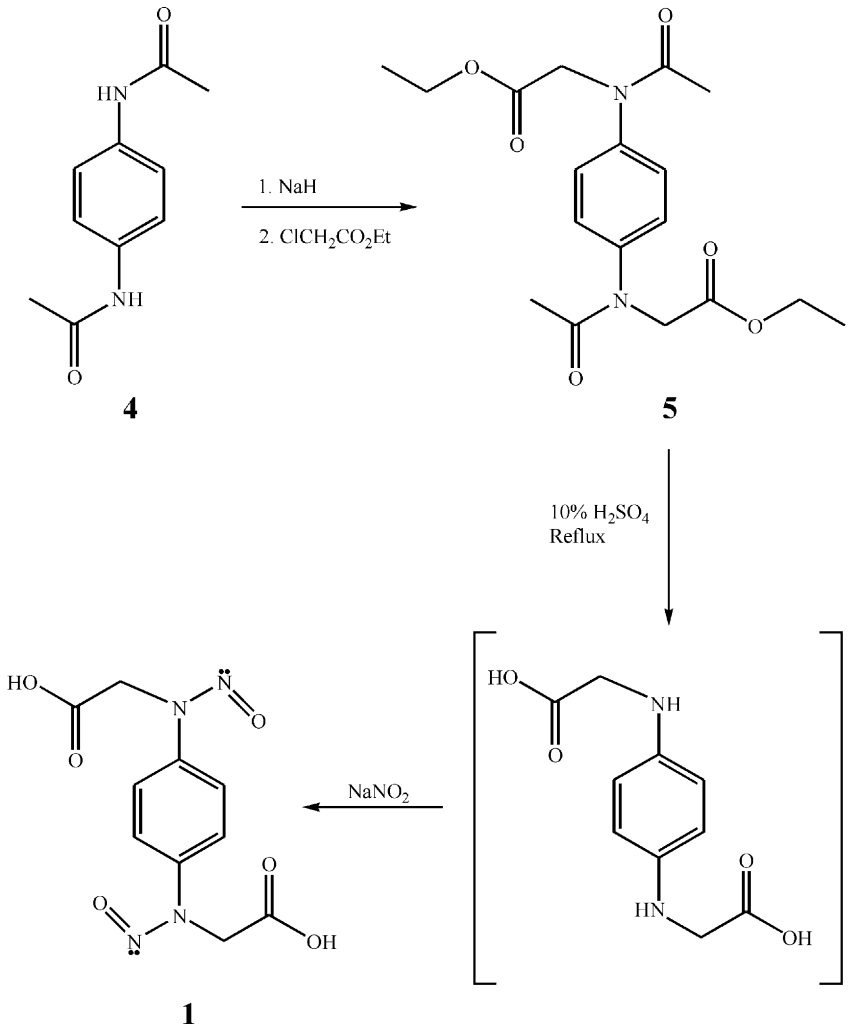


Scheme 2.

buffer, pH = 7.4): (300, 13, in agreement with literature value); (217, 13) [14]. $^1$H NMR ($\delta$, m, in $D_2O$/pH 7.55 phosphate buffer): 4.66, s, 4H of RN(NO)($CH_2$)$COO^-$; 7.70, s, 4H of Ph ring. Anal. Calcd. for $C_{10}H_{10}N_4O_6$: C, 42.53%; H, 3.57%; N, 19.85%. Found: C, 42.90%; H, 3.60%; N, 19.20%.

### 2.4. Laser spectroscopy, general setup

The configuration of the equipment used for the photogeneration and detection of transient species is illustrated in Fig. 1. In all cases the sample being investigated was held in a 2 mm × 10 mm fluorescence quartz cuvette (Hellma QS). Photochemistry was initiated with a single 10 ns pulse from a XeCl excimer laser (TUI, Existar 200), that crossed the 2 mm width of the cuvette. An Olis RSM-1000 spectrophotometer was used to monitor the absorbance changes induced by the laser pulse; the probe beam traversed the 10 mm length of the cuvette, at right angles to the laser pulse. UV sharp-cut filters (CVI Laser, CG-WG-320-1.00, 3 mm thickness) were used to protect the spectrophotometer's sample and reference photomultiplier tubes from the full intensity of light scattered from the laser pulse.[1] No lenses were used to focus the laser pulse onto the cuvette, but two mirrors allowed the pulse to be directed (Fig. 1). An adjustable slit, placed between the laser and the sample cuvette, was used to control the width of the laser pulse hitting the cuvette. The magnitude of the absorbance change elicited in the cuvette increased linearly with the slit width, up to a slit width of 5 mm. Thus, for the purpose of applying the Beer–Lambert law, the slit width determines the path length of the species photogenerated within the cuvette, for slit widths up to 5 mm wide.

[1] The 308 nm laser pulses induce fluorescence in the filters, and to a lesser extent in the reaction mixtures and the cuvette. Thus, despite the precaution taken to filter the laser pulses, a significant transient artifact, due to overload of the sample PMT by the fluorescence, was invariably detected in the spectrophotometric trace. This transient artifact decayed exponentially with a characteristic rate constant of about $1.75 \times 10^5\ s^{-1}$, and had an amplitude proportional to the intensity of the laser pulse.

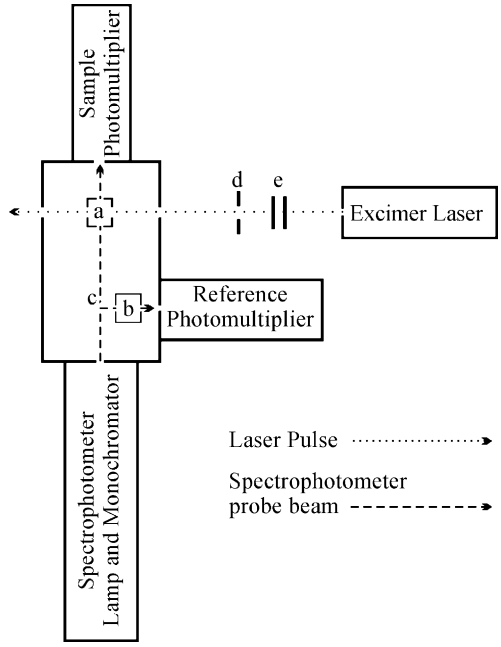


Fig. 1. Configuration of the equipment used for photogeneration of NO and detection of transient species. (a) Sample cell compartment; (b) reference cell compartment; (c) beamsplitter; (d) adjustable slit; (e) mirrors. For all of the experiments described in this paper, the laser energy output was fixed at 6.0 mJ/pulse, and the slit width was 5.0 mm.

### 2.5. Laser spectroscopy, sample handling

All laser flash photolysis experiments described in this paper were carried out in 50 mM phosphate buffer, pH = 7.4.[2] In agreement with previous investigators' results [14], we found that the spectrophotometric changes that followed the flash photolysis of **1** were unaffected by air, at least on the microsecond timescale and in the absence of added NO. Thus, such experiments were subsequently carried out aerobically. Experiments conducted in the presence of added NO had to be performed in anaerobic cuvettes (as described below) to avoid significant side reactions due to oxygen. In general, experiments were repeated multiple times, and their results averaged to improve the signal-to-noise ratio. Because a given sample was usually significantly and irreversibly altered by a single laser pulse, fresh sample was used in each replicate experiment. Experiments carried out under a NO atmosphere (see below) were an exception; under these conditions virtually all of the **2** and NO produced by the laser pulse recombined to give **1**, and so each experiment resulted in only minimal changes to the reaction mixture. Under these conditions it was possible to use the same sample for repeated flash photolysis experiments.

Nitric oxide for the experiments carried out under a NO atmosphere was supplied by Matheson (CP grade, 99.5%), and was handled in an all-glass vacuum line, connected to the gas cylinder by a stainless steel regulator and copper tubing (refrigeration grade). The NO gas was scrubbed using a column of NaOH pellets, to remove traces of other $NO_x$ compounds [20,21].[3] The total pressure within the vacuum line was monitored using a U-tube mercury manometer, read to within <0.2 mm with the aid of a cathetometer; standard corrections to the measured pressure were applied [22]. All experiments under NO were carried out in a tonometer fitted with a 2 mm × 10 mm fluorescence cuvette, at 20.5 ± 0.5 °C. Samples (vol. = 0.5 ml) were thoroughly degassed in the tonometer using four freeze/pump/thaw cycles then, with the stopcock between the tonometer and the vacuum line closed, the vacuum line was filled with roughly the desired pressure of NO. The stopcock to the tonometer was opened for about 3 s to introduce the NO, and then immediately closed again. The total pressure in the line at this point was taken to be the total pressure in the tonometer; $p_{NO}$ was obtained from the total pressure by correcting for the partial pressure of water within the tonometer at the recorded temperature [23].

### 2.6. Data analysis

Non-linear least-squares fitting of experimental data was generally performed using an implementation of the Levenberg–Marquardt algorithm, provided as part of the Microcal Origin (Version 6.0) package for data processing and display. Where data had to be fitted using numerical integration, we used a Quick Basic program that combined a Runge–Kutta integration routine with a Simplex multivariate minimization routine [24,25]; the code for this program is supplied as Supporting Material.

## 3. Results and discussion

Eq. (1) is the rate law expected according to the mechanism depicted in Scheme 1:

$$-\frac{d[\mathbf{2}]}{dt} = (k_r[NO] + k_d)[\mathbf{2}] \quad (1)$$

This rate law implies that at sufficiently low [NO] the $k_d$ term will predominate over the $k_r$[NO] term, and the disappearance of **2** will appear to be first order, with $k_{obs} \approx k_d$. Similarly at sufficiently high [NO] the disappearance of **2** should be pseudo first-order, with $k_{obs} = k_r[NO] + k_d$. Based on such an analysis, previous investigators obtained a value of $k_r = 1.38 \times 10^8\ M^{-1}\ s^{-1}$ in experiments performed under a NO atmosphere; by fitting only the late portion of a

[2] In a separate series of experiments not described here, the photochemical experiments were carried out in tris, bis–tris and phosphate buffers with pH values ranging from 6.2 to 9.5. No difference in reactivity was observed at the different pH values.

[3] Solutions of phosphate buffer placed under un-scrubbed NO showed distinct UV signals at 355 nm ($\varepsilon = 22.4\ M^{-1}\ cm^{-1}$) and 208 nm ($\varepsilon = 5110\ M^{-1}\ cm^{-1}$), due to nitrite produced by oxidation of $NO_x$ impurities in solution. These signals were completely absent when scrubbed NO was used.

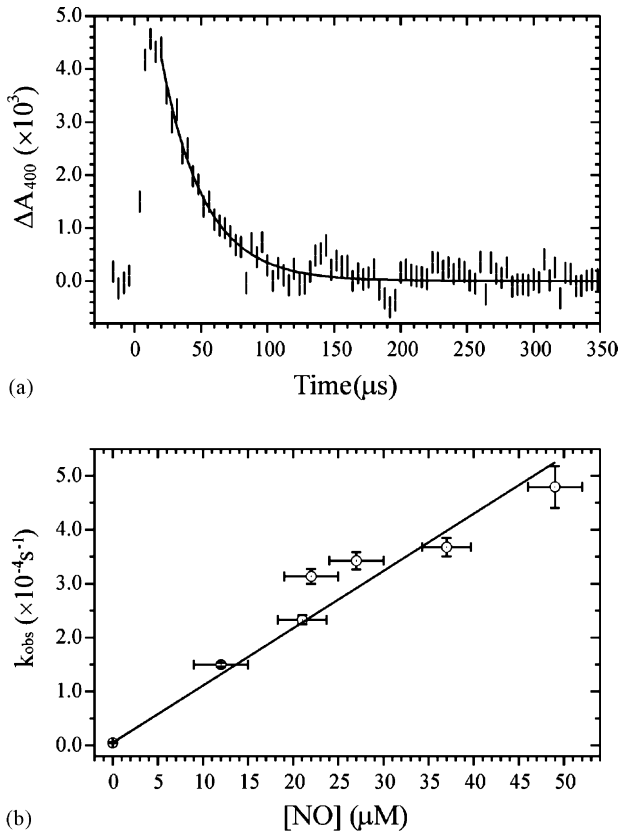


Fig. 2. (a) Kinetic trace (signal average of 25 replicates) obtained at 400 nm upon photoexcitation of a solution containing 0.1 mM of **1**, under $p_{NO} = (1.1 \pm 0.1) \times 10^{-2}$ atm ([NO] = 22 ± 3 μM); the laser pulse intensity was attenuated to 10% of full power by placing a filter between the laser and the sample. In this and all other kinetic traces, the error bars are estimated from the absorbance variation prior to the laser flash. The solid line indicates a single exponential fit, with $t_\infty$ fixed at zero. (b) Dependence of the rate constant $k_{obs}$, obtained in a series of experiments analogous to that depicted in (a), on [NO]. The value of $k_{obs}$ for [NO] = 0 was fixed at 500 $s^{-1}$ on the basis of the experiments described in Fig. 3, using the procedure described in the text.

kinetic trace that did not otherwise decay exponentially, they also obtained a value of $k_d = 2.96 \times 10^4\ s^{-1}$ [14].

Fig. 2a shows a typical $A_{400}$ vs. time trace obtained for a solution of **1** under NO gas ($p_{NO} = 1.1 \times 10^{-2}$ atm), fitted with a single exponential (further examples are supplied as Supporting Material). Fig. 2b shows a plot of $k_{obs}$ vs. [NO] obtained from a series of such experiments, performed under NO partial pressures varying between $5.9 \times 10^{-3}$ and $2.2 \times 10^{-2}$ atm (the final assignment of the intercept at [NO] = 0 is discussed below). At higher NO partial pressures the reaction rate was too fast to be observed with the available instrumentation. In all the experiments of Fig. 2b, the laser pulses were attenuated to 10% of the maximum attainable intensity. This ensured that the [NO] generated by dissociation of **1** could be neglected compared to the [NO] added in the gaseous form, and thus that the pseudo first-order limiting condition $k_{obs} = k_r[NO] + k_d$ was obtained. The data in Fig. 2b display the expected linear relationship between the parameters $k_{obs}$ and [NO]. However, the parameters $k_r$ and $k_d$ obtained by fitting the data to a straight line differ substantially from those previously reported [14]. Initially the slope of the line ($k_r$) was found to be $(8 \pm 1) \times 10^8\ M^{-1}\ s^{-1}$, while the intercept ($k_d$) was $(8 \pm 4) \times 10^3\ s^{-1}$. This $k_r$ value is ∼6× higher than the previously reported value while the $k_d$ value is ∼4× lower. The large uncertainties in the two values arise primarily from the measurement errors associated with the NO concentration at low $p_{NO}$, although for the fastest reactions the error in the measured value of $k_{obs}$ also becomes significant. Considerably more precise values of $k_r$ and $k_d$ were later obtained on the basis of the analysis described in the following paragraphs, and these are the values that were used to generate the line shown in Fig. 2b.

Fig. 3 shows three of six traces obtained by irradiating solutions of varying concentrations of **1** with full-intensity laser pulses (6 mJ/pulse), in the absence of added gaseous NO (the remaining three traces are supplied as supporting

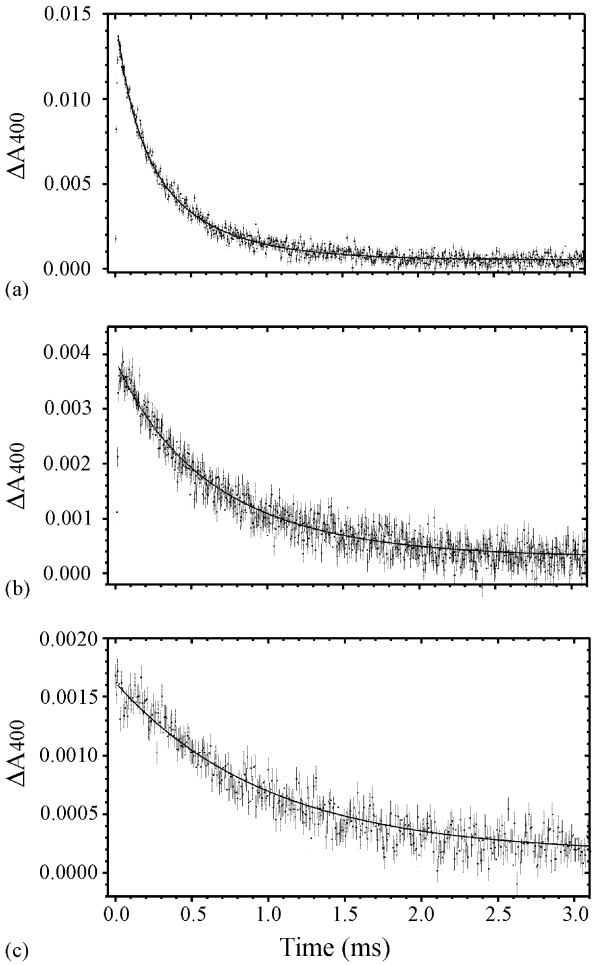


Fig. 3. Representative kinetic traces obtained at 400 nm upon photoexcitation of solutions containing: (a) 10.1 μM (signal average of 17 replicates), (b) 2.5 μM (signal average of 33 replicates) and (c) 1.35 μM (signal average of 50 replicates) of **1**. These traces and three additional traces given as Supporting Material were simultaneously fitted with Eq. (1), as described in the text. The theoretical fits are shown as solid black curves.

material). Visual inspection reveals that the half-lives for the decay in $A_{400}$ of the six traces range from 300 to 600 μs. This is immediately striking, because the published value of $k_d$ ($2.96 \times 10^4\ s^{-1}$) would fix the shortest obtainable half-life for the disappearance of **2** at 23 μs, an order of magnitude shorter than the shortest half life just mentioned. Indeed, these half-lives indicate that the true $k_d$ value is even lower than the $8 \times 10^3\ s^{-1}$ value obtained in the initial analysis of the data in Fig. 2b, which corresponds to a half-life of 87 μs (see previous paragraph). To obtain a more precise estimate of $k_d$ (and also, as a consequence, of $k_r$), the following procedure was used to analyze the data depicted in Figs. 2 and 3 together, in an iterative way. To begin with, all six traces obtained in the absence of added gaseous NO were simultaneously fitted to Eq. (1) using numerical integration (see Supporting Material) [25],[4] subject to the following constraints. First, $k_r$ was fixed at $8 \times 10^8\ M^{-1}\ s^{-1}$, on the basis of the results obtained under NO gas (Fig. 2). Second, three parameters: $k_d$, the extinction coefficient for **2** ($\varepsilon_{2(400)}$) and an extinction coefficient for an absorbing species present at $t_\infty$ ($\varepsilon_{f(400)}$, possibly **3**, but see below), were left as adjustable, but constrained to be the same in all experiments. Finally, the initial concentrations of **2** and NO ($[\mathbf{2}]_0 = [NO]_0$) were left as adjustable parameters, different for each individual run. Once a value of $k_d$ had been obtained from the iterative numerical integration process just described, it was then used as a fixed parameter to re-analyze the data shown in Fig. 2b, and obtain a new value for $k_r$. This $k_r$ value was in its turn used to re-analyze the data of Fig. 3. Within two cycles of this procedure the values of $k_r$ and $k_d$ converged to $(1.1 \pm 0.1) \times 10^9\ M^{-1}\ s^{-1}$, and $k_d$ to $500 \pm 50\ s^{-1}$, with corresponding values $\varepsilon_{2(400)} = (6.5 \pm 0.6) \times 10^3$, and $\varepsilon_{f(400)} = (1.4 \pm 0.1) \times 10^3\ M^{-1}\ cm^{-1}$. The values obtained in each experiment for $[NO]_0$ (or $[\mathbf{2}]_0$) as a function of [**1**], and for $[NO]_f$ (the concentration of NO at $t_\infty$) as a function of $[NO]_0$, are plotted in Fig. 4. The theoretical data obtained in the final iterative fit of the data in Fig. 3 are plotted as solid lines in Fig. 3, and are seen to be in excellent agreement with the experimental data under all the reaction conditions employed in this study.[5]

As earlier surmised in the visual inspection of Fig. 3, the calculated value of $k_d$ is much lower than the previously published estimate [14]. A possible explanation of this can be seen by analyzing Fig. 5, which shows simulated

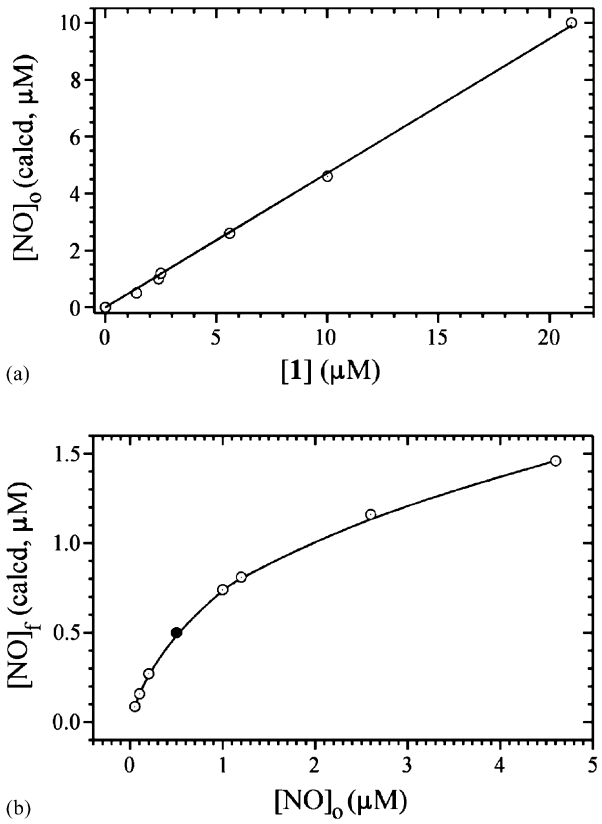


Fig. 4. (a) Concentration of NO immediately after the laser flash ($[NO]_0 = [\mathbf{2}]_0$), as a function of [**1**], calculated by fitting data sets such as those in Fig. 3 to Eq. (1). The data is fitted to a line with slope = 0.47, and intercept fixed at zero. (b) Relationship between [NO] at $t_\infty$ ($[NO]_f$) and $[NO]_0$, as calculated by numerical integration of Eq. (1) (and the corresponding equations for d[NO]/d*t* and d[**3**]/d*t*) for various selected values of $[NO]_0$. The solid data point indicates the point at which d[NO]/d*t* = 0, so that [NO] remains constant throughout.

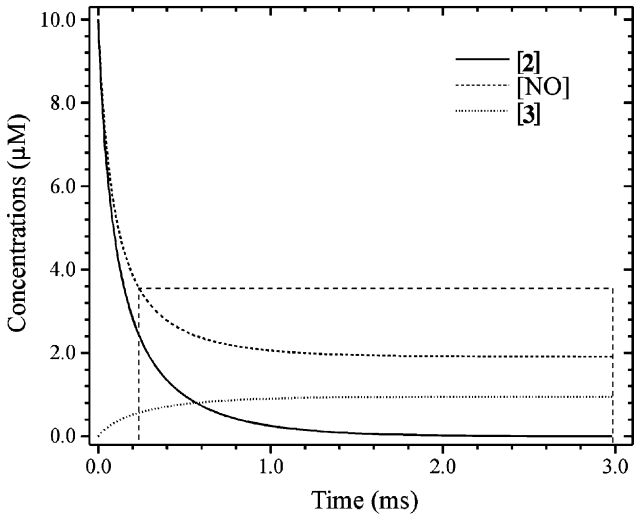


Fig. 5. Simulated traces of [**2**], [NO] and [**3**] as a function of time, obtained by numerically integrating Eq. (1) (and the corresponding equation for d[NO]/d*t*), with $[\mathbf{2}]_0 = [NO]_0 = 10\ \mu M$. The region within the dashed box is discussed in the text.

[4] In addition to the results reported here, excellent fits with Eq. (1) were also obtained for experiments in which [**1**] remained constant, but the laser flash intensity was attenuated to varying degrees. However, regardless of the experimental procedure employed, the fits were good only if conditions were such that $[\mathbf{2}]_0$ and $[NO]_0$ were not much greater than 10 μM. In experiments in which $[\mathbf{2}]_0$ and $[NO]_0$ were significantly greater that 10 μM, we observed that fits to Eq. (1) grew progressively poorer. We have some evidence that dimerization of **2** becomes a factor under these conditions, and are actively investigating this possibility at present.

[5] See Footnote 4.

traces for [NO], [**2**] and [**3**] vs. $t$, obtained by numerically integrating Eq. (1) (and the corresponding equations for d[NO]/d$t$ and d[**3**]/d$t$) [24,25], with $[NO]_0 = [\mathbf{2}]_0 = 10\,mM$. Initially [NO] decreases rapidly, as does [**2**]; however, in the region enclosed by the dashed box, as [**2**] continues to decrease to zero, note that [NO] changes by less than 50%. This indicates that during this time the quantity $k_r[NO] + k_d$ in Eq. (1) will not change by much either, and suggests that real data, with associated error bars, would be reasonably well fitted by a single exponential, even though [NO] is technically changing. However, the $k_{obs}$ thus obtained would *not* be $k_d$, it would be roughly $k_r[NO]_{av} + k_d$, where $[NO]_{av}$ is the average NO concentration over the region of the graph fitted. This analysis demonstrates the necessity for determining $k_d$ from multiple experiments, carried out under conditions which generate varying amounts of ($[\mathbf{2}]_0$, $[NO]_0$), rather than relying on a single data set. This is true even if the single data set can be fitted by a single exponential.

Fig. 4a shows that $[NO]_0$ (and $[\mathbf{2}]_0$) increase linearly with [**1**], and that nearly 50% of **1** in solution has dissociated at the time of the first measurement (the slope of the line in Fig. 4 is 0.47). Namiki et al. [14,17] have shown that substantial solvent cage radical recombination occurs between NO and **2** in the sub-μs timescale, so under the conditions reported here the initial yield of NO and **2** from **1** was probably close to 100%. The plot in Fig. 4b shows the amount of NO present at $t_\infty$ ($[NO]_f$) as a function of $[NO]_0$ or $[\mathbf{2}]_0$, as calculated by numerical integration of Eq. (1), and the corresponding equation for d[NO]/d$t$ [24,25]. Note that for $[NO]_0 = 0.5\,\mu M$ (highlighted point in Fig. 4b), $[NO]_0 = [NO]_f$; indeed, at this concentration [NO] is constant throughout, because $k_r[NO]_0 = k_d$, so that d[NO]/d$t$ = 0. For $[NO]_0$ greater than 0.5 μM [NO] decreases over time from $[NO]_0$, whereas at $[NO]_0$ lower than 0.5 μM it increases, approaching the theoretical maximum of $2[NO]_0$.

The magnitude of the extinction coefficient that we calculated for **2** ($\varepsilon_{2(400)} = 6500\,M^{-1}\,cm^{-1}$) is comparable to that reported by Namiki et al. [14]. However, inspection of the traces in Fig. 3 reveal a feature not mentioned in the earlier paper, namely that $A_{400}$ does not return to zero as $t \rightarrow \infty$ ($A_{400}$ does return to zero in the presence of excess NO, as seen in Fig. 2a, presumably because under these conditions all of **2** recombines with NO to generate **1**). Moreover, analysis of the visible spectrum between 390 and 600 nm a few milliseconds after photolysis of **1** indicates the presence of a species with noticeable absorbance all across the visible spectrum, and a maximum around 410 nm (Fig. 6). Although spectroscopically similar to **2**, this species is kinetically inert, remaining unchanged for at least 30 s after the laser flash. This observation is puzzling because, according to its published UV/Vis spectrum, the expected reaction product **3** should have no discernible absorbance at 400 nm [14]. One possible explanation is that the published UV/Vis spectrum of **3** was obtained in 0.1% aqueous phosphoric acid, and may be different at neutral pH. A second possible explanation is that in the presence of an excess of **1** the end-product **3** may form a colored transient charge-transfer complex, much like mixtures of quinone and hydroquinone do in the solid state [26]. The transient flash of intense pink observed during the synthesis of **1** from **5** may be due to the same type of phenomenon, and may thus provide preliminary evidence that this type of chemistry can occur with phenylenediamine-based compounds. Further studies are currently under way to better understand the origins of the visible absorbance seen both in the kinetic investigations (Figs. 7 and 8) and during the synthesis.

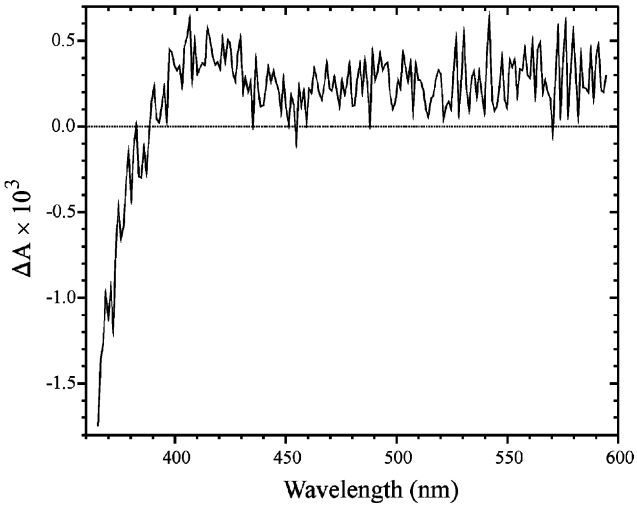


Fig. 6. Difference spectrum obtained 3 ms after irradiation of a sample of **1** with a laser pulse. Under the conditions of this experiment, $[\mathbf{2}]_0$ (=$[NO]_0$) was 2.5 μM.

## 4. Conclusion

We have re-investigated the reactions that follow the laser-induced flash photolysis of **1** into **2** and NO (Scheme 1), under conditions in which $[\mathbf{2}]_0$ and $[NO]_0$ do not exceed about 10 μM. Under these conditions recombination of **2** with NO, and dissociation of an additional equivalent of NO from **2** to form **3** (Scheme 1), appear to be the dominant pathways leading to the depletion of **2**, as had been proposed earlier by Namiki et al. [14].[6] In the present study, the rate constant $k_r$ that governs the recombination of **2** with NO to regenerate **1** (Scheme 1) was found to have a value of $(1.1 \pm 0.1) \times 10^9\,M^{-1}\,s^{-1}$, while the rate constant $k_d$ governing the dissociation of the second equiv of NO from **2** was found to be $500 \pm 50\,s^{-1}$. Both of these values are significantly different from the values reported earlier by Namiki et al. [14], based on a less detailed kinetic analysis. The present analysis also revealed the previously unre-

[6] See Footnote 4.

ported presence of an absorbing species at $t_\infty$, which may be **3** (Scheme 1) but could also be a charge-transfer complex of **1** and **3**. Further investigations of this feature are currently under way. We are now also investigating situations in which concentrations of **2** and NO in large excess of 10 μM are generated by the initial photolysis of **1**,[7] in order to extend the range of conditions under which the versatile NO-generating species **1** can be used in quantitative experiments.

## Acknowledgements

We thank Kevin Newby for technical assistance, Alan Schwabacher for valuable and helpful discussions, and Gordon Tollin, James Hazzard and John Hurley for proof-reading the manuscript and providing helpful suggestions. Financial support received from the University of Wisconsin-Milwaukee Graduate School is gratefully acknowledged.

## Appendix A. QUICKBASIC 4.5 code for fitting data to Eq. (1)

Given initial guesses for $k_r$, $k_d$, $\varepsilon_{2(400)}$, $\varepsilon_{f(400)}$ and initial concentrations of NO ($[NO]_0$), the following program iteratively fits a series of data sets with varying $[NO]_0$ to obtain the best estimates of the parameters. Note that $k_r$ and $\varepsilon_{2(400)}$ are completely correlated, and one or the other must be fixed on the basis of other experiments. Here, $k_r$ was fixed on the basis of experiments performed at high [NO] (see text). The program takes the user-supplied initial parameter estimates and calls on the numerical integrator RKDUMB to generate $A_{400}$ vs. $t$ (s) data corresponding to each of the experimental data sets. RKCHI2 then compares the theoretical and experimental data, and calculates a $\chi^2$ value corresponding to each parameter set. The parameter sets, together with their corresponding $\chi^2$ values, are then sent to the simplex multivariate minimization routine AMOEBA, which generates new parameter sets for the integrator to use. The program continues until the $\chi^2$ values cluster around a minimum value. The programs RKDUMB and AMOEBA were taken directly from [25].

```
DECLARE SUB ABSSIM (MP!, PARAMS!())
DECLARE SUB RKDUMB (VSTART!(), NVAR!, X1!,
  X2!, NSTEP!, DUM!)
DECLARE FUNCTION RKCHI2! (PARAMS(), NP)
DECLARE FUNCTION AMOEB! (X!(), NP!)
DECLARE SUB AMOEBA (P!(), Y!(), MP!, NP!, NDIM!,
  FTOL!, DUM!, ITER!)
COMMON SHARED XX(), Y()
COMMON SHARED YDAT(), SDEV(), Absor(),
  NDATA(), PDATA(), Deadtime()
COMMON SHARED pathlength, DSETS
COMMON SHARED STARTPOINT(), kd, kr, EBNN
    This program is used to analyze experiments in which
  NO is generated from BNN5Na. Corrected to account for
  loss of BNN5Na at t = 0.
CLS
```

First we want to load up the experimental data sets that will be fitted with theoretical curves by the program:

```
INPUT "How many datasets do you want to fit?", DSETS
We need to specify arrays in which to store the data:
DIM XDAT(DSETS, 2000), YDAT(DSETS, 2000),
  SDEV(DSETS, 2000), Absor(DSETS, 2000)
DIM NDATA(DSETS), PDATA(2, DSETS), Dead-
  time(DSETS), STARTPOINT(2, DSETS)
```

SDEV will store the errors associated with the data, NDATA will store the total number of data points in each set, and PDATA will store the time interval between successive data points, and the number of data points collected after the laser flash (i.e.: with $t$-values >0). Absor will store the theoretical absorbance values generated by the integrator, and deadtime will store the experimentally determined deadtime of the instrument, which will depend on the laser intensity, and the magnitude of the flash artifact.

```
INPUT "Supply the path to where the data files are stored:",
  PATH$
DIM FINFILE$(DSETS)
FOR I = 1 TO DSETS
  INPUT "Input the name of the file containing the data
    to be fitted:", FILE$
  FINFILE$(I) = PATH$ + FILE$
  FILE$ = PATH$ + FILE$ + ".dat"
  OPEN FILE$ FOR INPUT AS #I
  KOUNT = 1
  DO UNTIL EOF(I)
    INPUT #I, XDAT(I, KOUNT), YDAT(I, KOUNT),
      SDEV(I, KOUNT)
    IF XDAT(I, KOUNT) = 0 THEN
      PDATA(2, I) = KOUNT   ' This stores the #
        of data pts up to the flash
    END IF
    KOUNT = KOUNT + 1
  LOOP
  KOUNT = KOUNT - 1
  NDATA(I) = KOUNT      This stores the total #
      of points
  IF I = 1 THEN      Store the dead-times here...
    INPUT "What is the dead-time for this run
      (in seconds)?", Deadtime(1)
  ELSE
```

[7] See Footnote 4.

```
    INPUT "What is the dead-time for this run?
      (type s if the same as prev)", DUM$
    IF DUM$ = "s" THEN
      Deadtime(I) = Deadtime(I–1)
    ELSE
      Deadtime(I) = VAL(DUM$)
    END IF
  END IF
  PDATA(1, I) = XDAT(I, 2)—XDAT(I, 1)
    This calculates the # of data points
  PDATA(2, I) = NDATA(I)—PDATA(2, I)
    after the flash, and interval bet points
  CLOSE #I
NEXT I
```

The parameters that will be optimized by AMOEBA are the rate constants (kd and kr), the initial concentration of NO and MNN5Na (Yo), and the extinction coefficients of MNN5Na and its decomposition product (Eo and Ef). In addition, the path length and extinction coefficient of BNN5Na at the measuring wavelength are supplied as a known parameters kd, kr, Eo and Ef are the same for all data sets. On the other hand, each data set will be associated with a unique value of Yo. Therefore, the number of parameters (NPAR) required for the fitting will be:

$$\mathrm{NPAR} = 4 + \mathrm{DSETS}$$

The initial guesses for these parameters are stored in array P(1 + DSETS, DSETS):

```
MP = NPAR + 1      Number of initial guesses
NP = NPAR      Number of adjustable parameters
FTOL = 0.0001      This parameter controls the termination criteria for AMOEBA
DIM P(MP, NP), PTEST(NP), CHISQ(MP)      PTEST() will carry individual parameter sets to the next program, while
  CHISQ() will store the resulting Chi square values
DIM FX(NP)
INPUT "First guess for kd, kr, Eo and Ef?", P(1, 1), P(1, 2), P(1, 3), P(1, 4)
PRINT "You may choose to leave some of these parameters fixed."
PRINT "Enter in the order kd, kr, Eo, Ef, a 0 to fix, or a 1 to adjust:"
INPUT; FX(1), FX(2), FX(3), FX(4)
FOR I = 5 TO NP
  FX(I) = 1
NEXT I
FOR J = 1 TO DSETS
  INPUT "What is your guess for the next Yo value?", P(1, 4 + J)
NEXT J
INPUT "What are the pathlength and extinction coefficient of BNN5Na?", pathlength, EBNN
FOR I = 2 TO MP      This loop calculates additional guesses orthogonal to the first.
  FOR J = 1 TO NP
    IF J = I—1 THEN
      IF FX(J) = 1 THEN
        P(I, J) = 1.1 * P(1, J)
      ELSE
        P(I, J) = P(1, J)
      END IF
    ELSE
      P(I, J) = P(1, J)
    END IF
  NEXT J
NEXT I
FOR I = 1 TO MP
  FOR J = 1 TO NP
    PTEST(J) = P(I, J)
  NEXT J
  CHISQ(I) = AMOEB(PTEST(), NP)
NEXT I
CALL AMOEBA(P(), CHISQ(), MP, NP, NP, FTOL, DUM, ITER)
```

```
DIM FINALPARS(NP)
FOR I = 1 TO NP
  FOR J = 1 TO MP
    FINALPARS(I) = FINALPARS(I) + P(J, I)
  NEXT J
  FINALPARS(I) = FINALPARS(I)/MP
NEXT I
PRINT
PRINT "Final Parameter Values and Chi-Square:"
PRINT
PRINT "kd ="; FINALPARS(1)
PRINT "kr ="; FINALPARS(2)
PRINT "Eo ="; FINALPARS(3)
PRINT "Ef ="; FINALPARS(4)
FOR I = 1 TO DSETS
  PRINT "Initial conc"; I; "="; FINALPARS(4 + I)
NEXT I
CHIFIN = 0
FOR J = 1 TO MP
  CHIFIN = CHIFIN + CHISQ(J)
NEXT J
CHIFIN = CHIFIN/MP       Average Chi-square
PRINT "Chi-square =";
PRINT USING "##.###^^^^"; CHIFIN
NDATA = 0
DIM FITDATA(DSETS)
FOR J = 1 TO DSETS
  FITDATA(J) = (PDATA(2, J)—STARTPOINT(2, J) + 2)       # of pts. fitted per dset
  NDATA = NDATA + FITDATA(J)
NEXT J
PRINT "The total number of points fitted was:", NDATA
FOR I = 1 TO DSETS
  FILE2$ = FINFILE$(I) + "'.cal"
  OPEN FILE2$ FOR OUTPUT AS #I
  FOR J = 1 TO FITDATA(I)
    WRITE #I, XDAT(I, J − 1 + STARTPOINT(1, I)), Absor(I, J − 1 + STARTPOINT(2, I)), (YDAT
      (I, J − 1 + STARTPOINT(1, I))—Absor(I, J − 1 + STARTPOINT(2, I)))
  NEXT J
  CLOSE #I
NEXT I
END
SUB ABSSIM (MP, PARAMS!())
NVAR = 4
kd = PARAMS(1)
kr = PARAMS(2)
Eo = PARAMS(3)
Ef = PARAMS(4)
X1 = 0       All integrations will start at t = 0
FOR I = 1 TO DSETS
  X2 = PDATA(1, I) * PDATA(2, I)       Calc what time value to integrate to...
  NSTEP = PDATA(2, I)       ... and store the number of steps to be taken
  DIM VSTART(NVAR), XX(NSTEP + 1), Y(NVAR, NSTEP + 1)
```

```
VSTART(1) = PARAMS(4 + I)       trial initial conc of MNN5Na,
  VSTART(2) = PARAMS(4 + I)       and of NO. . .
  VSTART(3) = 0       and of the MNN5Na decomposition product
  VSTART(4) = -PARAMS(4 + I)       and the depletion of BNN5Na by the flash
  CALL RKDUMB(VSTART(), NVAR, X1, X2, NSTEP, DUM)       Now calculate the corresponding absorbance traces
  FOR J = 1 TO NSTEP + 1
    Absor1 = Eo * pathlength * Y(1, J)       Absorbance due to MNN5Na
    Absor2 = Ef * pathlength * Y(3, J)       Absorbance due to the MNN5Na decomposition prod.
    Absor3 = EBNN * pathlength * Y(4, J)       Negative absorbance due to BNN5Na depletion
    Absor(I, J) = Absor1 + Absor2 + Absor3
  NEXT J
  ERASE VSTART, XX, Y
NEXT I
END SUB
FUNCTION AMOEB (X(), NP)
FOR I = 1 TO NP
  IF X(I) < 0 THEN
    AMOEB = 1E + 09
    EXIT FUNCTION
  END IF
NEXT I
AMOEB = RKCHI2(X(), NP)
END FUNCTION
SUB DERIVS (X, Y(), DYDX())
DYDX(1) = -(kr * Y(1) * Y(2) + kd * Y(1))       Diff. eq. for MNN5Na disappearance
DYDX(2) = kd * Y(1)—kr * Y(1) * Y(2)       Diff. eq. for NO formation
DYDX(3) = kd * Y(1)       Diff. eq. for decomposition prod.
DYDX(4) = kr * Y(1) * Y(2)
END SUB
FUNCTION RKCHI2 (PARAMS(), NP)
CALL ABSSIM(NP, PARAMS())
CHI2 = 0
FOR I = 1 TO DSETS
  SKIP = CINT(Deadtime(I)/PDATA(1, I))
  STARTPOINT(1, I) = (NDATA(I)—PDATA(2, I)) + SKIP       First data pt fitted
  STARTPOINT(2, I) = SKIP + 1       Corresponding first calculated point
  FOR J = 1 TO (PDATA(2, I)—STARTPOINT(2, I))
    CHI2 = CHI2 + ((YDAT(I, J  −  1 + STARTPOINT(1, I))—Absor(I, J − + STARTPOINT(2, I)))/SDEV(I,
      J − 1 + STARTPOINT(1, I)))2̂
    IF CHI2 > 1E + 30 THEN
      CHI2 = 1E + 30
      EXIT FOR
    END IF
  NEXT J
  IF CHI2 > 1E + 30 THEN
    CHI2 = 1E + 30
    EXIT FOR
  END IF
NEXT I
RKCHI2 = CHI2
PRINT "RKCHI2 =", CHI2
END FUNCTION
```

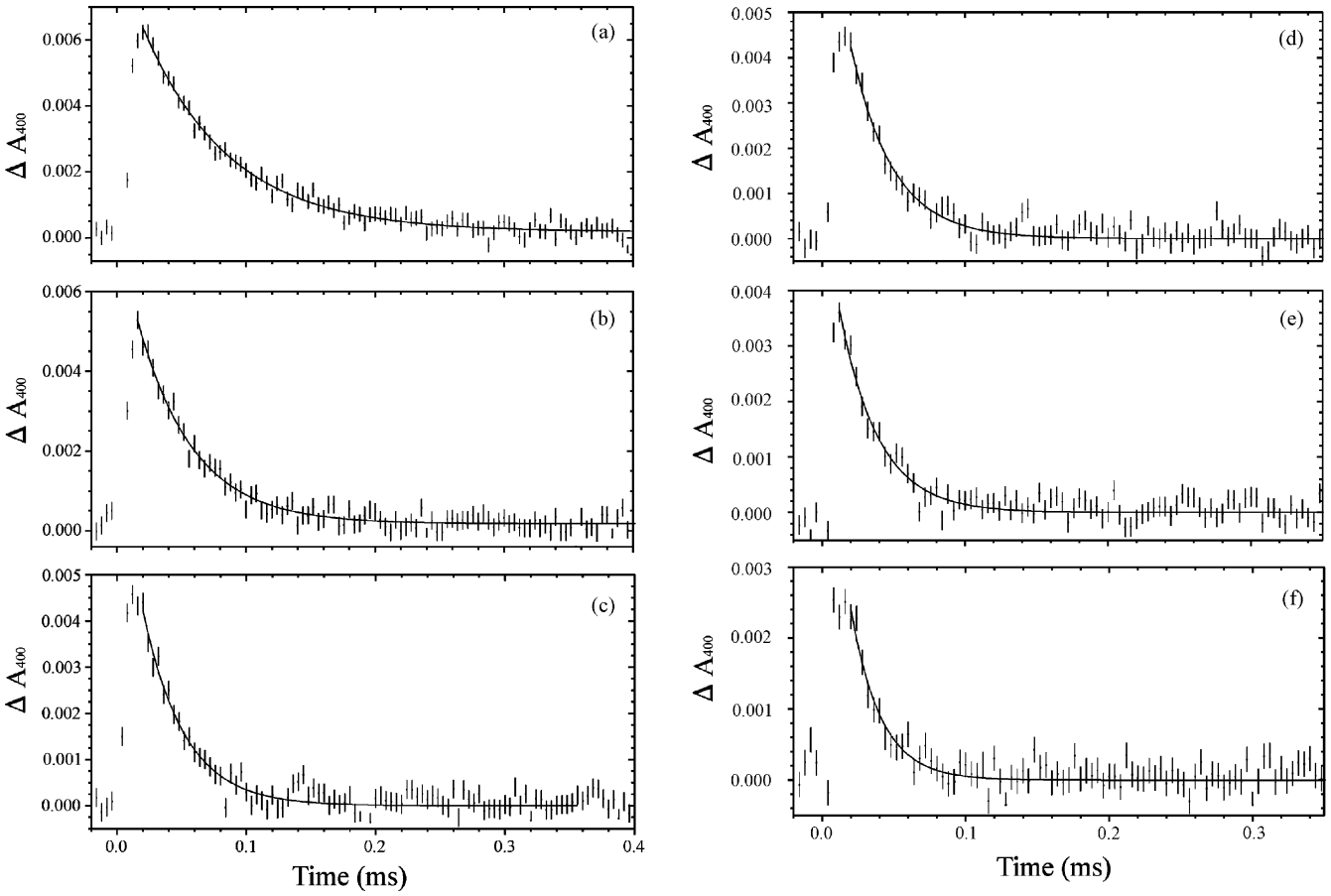


Fig. 7. Kinetic traces obtained at 400 nm upon photoexcitation of solutions containing 0.1 mM of **1**, under varying partial pressures of NO gas. In all cases the laser pulse intensity was attenuated to 10% of full power by placing a filter between the laser and the sample. The solid lines indicate single exponential fits. (a) $p_{NO} = (5.9 \pm 1.3) \times 10^{-3}$ atm, [NO] = 12 ± 3 μM; (b) $p_{NO} = (1.0 \pm 0.1) \times 10^{-2}$ atm, [NO] = 21 ± 3 μM; (c) $p_{NO} = (1.1 \pm 0.1) \times 10^{-2}$ atm, [NO] = 22 ± 3 μM; (d) $p_{NO} = (1.3 \pm 0.1) \times 10^{-2}$ atm, [NO] = 27 ± 3 μM; (e) $p_{NO} = (1.8 \pm 0.1) \times 10^{-2}$ atm, [NO] = 37 ± 3 μM; (f) $p_{NO} = (2.2 \pm 0.1) \times 10^{-2}$ atm, [NO] = 46 ± 3 μM. Fig. 2b was based on these data.

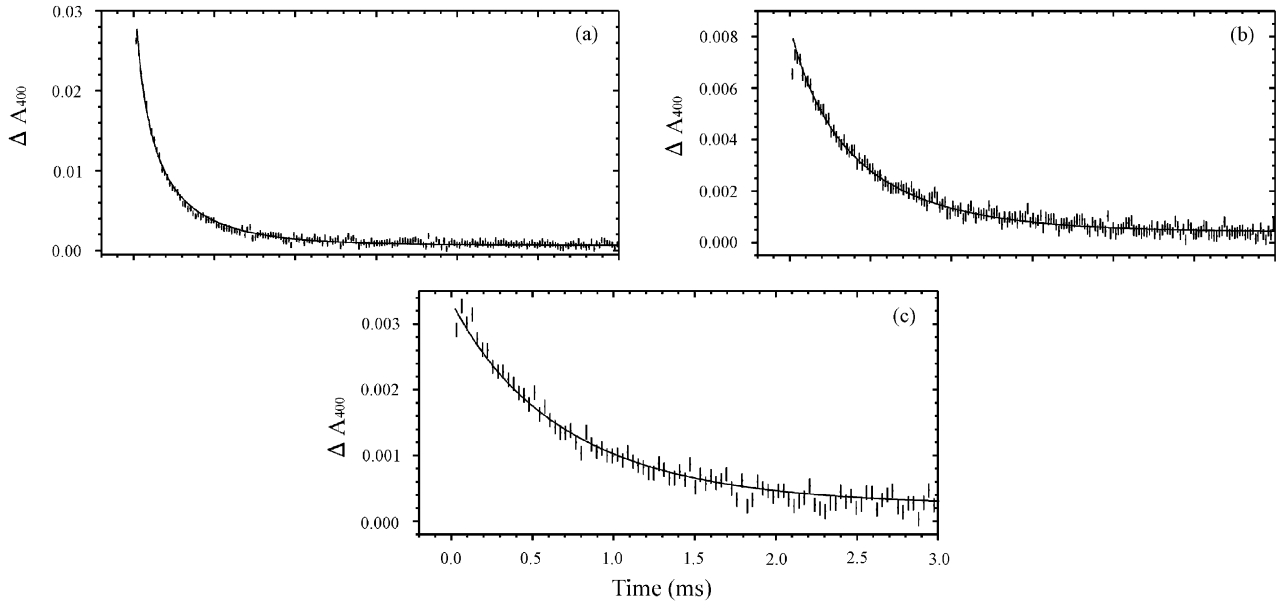


Fig. 8. Representative kinetic traces obtained at 400 nm upon photoexcitation of solutions containing: (a) 21.2 μM (signal average of 10 replicates), (b) 5.6 μM (signal average of 27 replicates) and (c) 2.4 μM (signal average of 51 replicates) of **1**. These traces and the traces shown in Fig. 3 were simultaneously fitted with Eq. (1), as described in the text. The theoretical fits are shown as solid black curves.

## References


[1] J.B. Hibbs, Z. Vavrin, R.R. Taintor, J. Immunol. 138 (1987) 550–565.
[2] S. Moncada, R.M.J. Palmer, E.A. Higgs, Biochem. Pharmacol. 38 (1989) 1709–1715.
[3] H. Bult, G.E. Boeckxstaens, P.A. Pelckmans, F.H. Jordaens, Y.M. Van Maercke, A.G. Herman, Nature 345 (1990) 346–347.
[4] K. Shibuki, D. Okada, Nature 349 (1991) 326–328.
[5] D.S. Bredt, P.M. Hwang, C.E. Glatt, C. Lowenstein, R.R. Reed, S.H. Snyder, Nature 351 (1991) 714–718.
[6] D.E. Heck, D.L. Laskin, C.R. Gardner, J.D.J. Laskin, Biol. Chem. 267 (1992) 21277–21280.
[7] M. Hoshino, M. Maeda, R. Konishi, H. Seki, P.C.J. Ford, Am. Chem. Soc. 118 (1996) 5702–5707.
[8] L.E. Laverman, M. Hoshino, P.C.J. Ford, Am. Chem. Soc. 119 (1997) 12663–12664.
[9] K.J. Franz, S.J.J. Lippard, Am. Chem. Soc. 120 (1998) 9034–9040.
[10] I.S. Zavarine, A.D. Kini, B.H. Morimoto, C.P.J. Kubiak, Phys. Chem. B 102 (1998) 7287–7292.
[11] G.B. Richter-Addo, Acc. Chem. Res. 32 (1999) 529–536.
[12] K.M. Davies, D.A. Wink, J.E. Saavedra, L.K.J. Keefer, Am. Chem. Soc. 123 (2001) 5473–5481.
[13] J. Bourassa, W. DeGraff, S. Kudo, D.A. Wink, J.B. Mitchell, P.C.J. Ford, Am. Chem. Soc. 119 (1997) 2853–2860.
[14] S. Namiki, T. Arai, K.J. Fujimori, Am. Chem. Soc. 119 (1997) 3840–3841.
[15] M. De Leo, P.C.J. Ford, Am. Chem. Soc. 121 (1999) 1980–1981.
[16] Y. Hou, W. Xie, A.J. Janczuk, P.G.J. Wang, Org. Chem. 65 (2000) 4333–4337.
[17] M. Yoshida, I. Masashi, S. Namiki, T. Arai, K. Fujimori, Chem. Lett. (2000) 730–731.
[18] S. Namiki, F. Kaneda, M. Ikegami, T. Arai, K. Fujimori, S. Asada, H. Hama, Y. Kasuya, K. Goto, Bioorg. Med. Chem. 7 (1999) 1695–1702.
[19] M.Z. Cabail, A.A. Pacheco, Inorg. Chem. submitted.
[20] V.G. Kharitonov, A.R. Sundquist, V.S.J. Sharma, Biol. Chem. 270 (1995) 28158–28164.
[21] C.T. Aravindakumar, J. Ceulemans, M. De Ley, Biochem. J. 344 (1999) 253–258.
[22] D.F. Shriver, M.A. Drezdzon, The Manipulation of Air-Sensitive Compounds, 2nd Edition, Wiley, New York, 1986, pp. 132–135.
[23] R.C. Weast, M.J. Astle (Eds.), CRC Handbook of Chemistry and Physics, 62nd Edition, CRC Press, Boca Raton, 1982, p. D-168.
[24] W.H. Press, S.A. Teukolsky, W.T. Vetterling, B.P. Flannery, Numerical Recipes in C: The Art of Scientific Computing, 2nd Edition, Cambridge University Press, Cambridge, 1992, pp. 408–412, 710–722.
[25] J.C. Sprott, Numerical Recipes Routines and Examples in BASIC, Cambridge University Press, Cambridge, 1991, pp. 225–228, 360–368.
[26] A. Streitwieser, C.H. Heathcock, Introduction to Organic Chemistry, 3rd Edition, Macmillan, New York, 1985, pp. 832–834.